Rock Mechanics Bulletin 5 (2026) 100223

Contents lists available at ScienceDirect

Rock Mechanics Bulletin

journal homepage: www.keaipublishing.com/en/journals/rock-mechanics-bulletin

Effects of loading rates and mine water immersion on the mechanical characteristics of coal under Brazilian test conditions

Xiaobin Li [a], Gan Feng [b,*], Xu Wang [c,d], Jianxiong Yang [b], Yu Zhao [e], Guifeng Wang [f], Mingli Xiao [b], Chunyu Gao [b], Huaizhong Liu [b]

[a] State Key Laboratory of Water Resource Protection and Utilization in Coal Mining, National Institute of Low Carbon and Clean Energy, Beijing, 102209, China
[b] College of Water Resource & Hydropower, Sichuan University, Chengdu, 610065, China
[c] China Railway Chuanzang Science and Technology Innovation Center (Chengdu) Co., Ltd., Chengdu, 610213, China
[d] Sichuan Tibet Railway Technology Innovation Center Co., Ltd., Chengdu, 610000, China
[e] College of Civil Engineering, Guizhou University, Guiyang, 550025, China
[f] School of mines, China University of Mining and Technology, Xuzhou, 221116, China

ARTICLE INFO

Keywords:
Coal
Underground water reservoir
Mechanical characteristics
Loading rate
Brazilian splitting

ABSTRACT

The mechanical properties of coal pillars are crucial for evaluating the stability of underground water reservoirs in coal mines. This article examines the fracture mechanical behavior of coal in response to mine water immersion, layer direction, and loading rate. Eight types of specimens were studied, featuring inclination angles between the applied force and the bedding plane of 0°, 15°, 30°, 45°, 60°, 75°, 90°, and the Divider type. The loading rates (V) tested were 0.005 kN/s, 0.02 kN/s, 0.05 kN/s, and 0.1 kN/s. The results indicated that after immersion in mine water for 30 days, the Brazilian splitting strength (BSS), splitting modulus (E_m), and absorbed energy (U_a) of coal decreased by 51.35%, 52.37%, and 44.60%, respectively, compared to the non-immersion samples. The primary reason for this phenomenon is that the production rate of micropores and small pores resulting from mine water immersion surpasses their conversion rate to mesopores and macropores. This imbalance leads to the fragmentation of the internal structure of coal and the interconnection of pore fracture zones, thereby significantly weakening its bearing capacity. It has been observed that the relative proportions of failure mechanisms along and across the bedding plane directly influence the variations in coal mechanical properties at different θ values. Additionally, BSS, E_m, and U_a of coal gradually increase with an increase in loading rate, which is due to the reduced duration of coal damage development and evolution, subsequently lowering the probability of activating weak structures.

1. Introduction

The extensive use of traditional fossil fuels can cause pollution to the environment (Zhang et al., 2025). The global energy structure is gradually transitioning towards renewable, green, and clean energy sources. However, wind and solar energy, as renewable sources, are challenging to dispatch due to their intermittency and volatility, making it difficult for their output to adapt to constantly changing demand (Hu et al., 2016; Mileva et al., 2016; Okazaki et al., 2015). Underground pumped storage hydropower stations (UPSH) can store excess energy and generate electricity during high demand periods (Bussar et al., 2016; Moriarty et al., 2016; Menéndez et al., 2019). Coal mine underground reservoirs represent ideal locations for pumped storage power generation (Colas et al., 2023). By utilizing the elevation differences between multiple underground water reservoirs in coal mines, pumped storage and discharge power generation systems can be constructed. This opportunity arises because coal, as a traditional energy source, has created numerous goaf and roadway spaces through long-term mining. The technology of underground water reservoirs in coal mines involves using these spaces and connecting the surrounding coal pillars with artificial dam bodies to form a reservoir dam structure (Kong et al., 2024). The complex coal rock layers and geostress in coal mines cause coal pillars to be subjected not only to pressure from overlying rock layers but also to lateral pressure from surrounding rocks and water along the bedding

* Corresponding author.
E-mail address: fenggan@whu.edu.cn (G. Feng).
Peer review under the responsibility of Chinese Society for Rock Mechanics & Engineering.

https://doi.org/10.1016/j.rockmb.2025.100223
Received 6 June 2025; Received in revised form 23 June 2025; Accepted 5 July 2025
Available online 17 July 2025

direction (Tang et al., 2019). When coal is under pressure, it undergoes lateral deformation due to Poisson's effect. Once this deformation reaches the mechanical limit that coal can withstand, the coal pillar becomes damaged. Consequently, the mechanical properties of coal pillars are a critical factor determining the stability of underground water reservoirs in coal mines (Bodeux et al., 2017).

Coal pillars are immersed in mine water for extended periods during the operation of underground reservoirs. Water is a primary factor influencing the physical and mechanical properties of coal rock (Yao et al., 2020a), which is evident in water-rock interactions. The interaction between water and rock leads to structural destruction through element migration and mineral transformation (Ling et al., 2015). Water induces the formation of microcracks and micropores in rocks, accelerating the development of subcritical cracks (Liu and Cao, 2016) and causing damage to the microstructure of rocks. This damage results in strength discrepancies between mineral particles, thereby reducing resistance to crack propagation within rocks (Maruvanchery et al., 2019). Additionally, water can promote the dissolution of certain organic matter and mineral components, weaken the bonding forces between particles, and generate stress corrosion effects that facilitate crack initiation, development, and propagation. However, mine water is a complex aqueous solution compared to pure water, typically exhibiting acidity, alkalinity, or high salt concentrations, which have a more intricate impact on coal than pure water.

In addition to the external environmental factor of mine water, the influence of the structure of the coal pillar dam on its mechanical properties is significant. Coal is not a homogeneous medium; its layered structure is quite pronounced. After coal mining, coal pillars serve to support the roof, leading to significant stress concentration. The relative position of bedding planes and stress concentration areas critically affects the stability of coal pillars. This is due to the bedding plane of coal being a weak plane, where the inclination angle between the bedding plane and the applied load can cause the weak plane to exhibit varying mechanical states in conjunction with the matrix and the applied load. Concentrated loads along the bedding plane can easily result in coal pillar instability. The strength anisotropy of coal is influenced by the distribution of microstructural directions. The bedding plane directly governs the uniaxial compressive strength of coal, and the presence of mineral inclusions enhances the heterogeneity of coal, creating significant variations in strength and deformation between mineral inclusion zones (Zhao and Song et al., 2019a). Song et al. (2018) found that the uniaxial compressive strength of coal exhibits a U-shaped variation curve with the dip angles of bedding planes (0°, 15°, 30°, 45°, 60°, and 90°). Sun et al. (2025) conducted a water immersion experiment on coal from the Daliuta Coal Mine in China for up to 16 days and found that the mechanical strength and elastic modulus of coal demonstrated significant anisotropy along different bedding planes. After immersion for 16 days, the strength of coal with vertical and horizontal inclination angles decreased by 29% and 45%, respectively. The study by Qian et al. (2024) showed that the peak strength of crushed coal first decreases and then increases as the crushing angle varies from 15° to 75°. The peak strength decreases with increasing water pressure, while the failure mode is shear failure.

It is important to note that coal pillars are subjected to varying loading rates from pumping, water storage, and disturbances caused by nearby coal seam mining, compounded by the long-term corrosion of coal from mine water. This results in complex loading rate effects on the stress state of coal pillars. The mechanical response of coal rock changes under different loading rates. The loading rate can alter the rock failure mode, and there exists a critical loading rate for the brittle-ductile transition during the failure process (Zhang et al., 2018). Shi et al. (2022) conducted notch semi-circular bending (NSCB) tests on anisotropic coal with different bedding angles (ranging from 0° to 90°) and found that the bedding effect diminished with increasing loading rates. Li et al. (2015) observed that strength initially increases and then decreases with rising loading rates, with the loading rate at the turning point termed the critical loading rate. Yang et al. (2023) identified that a loading rate of 0.01 mm/s is the critical loading rate leading to a turning point in the mechanical strength of saturated coal samples. The macroscopic failure mode of saturated coal samples at varying loading rates is predominantly characterized by tensile shear composite failure, primarily driven by shear failure.

From the aforementioned analysis, it is evident that the coal pillar dam body exists in a long-term corrosive environment caused by mine water. Additionally, it is affected by variable rate disturbances from adjacent coal seam mining, pumped hydro power generation, and water storage. The impact of the stress environment on the mechanical behavior of coal pillars is significant. Therefore, studying the mechanical response of coal under the combined effects of the physical and chemical environment of mine water and varying loading speeds is crucial. Previous studies have demonstrated that water intrusion promotes crack propagation and weakens the strength of the media (Chen et al., 2017; Sadeghiamirshahidi et al., 2019). While numerous reports have addressed the weakening effects of water on coal and rock, mine water contains more complex components than pure water. Currently, there is a lack of scientific research examining the impact of mine water on coal structure and the corresponding mechanical response characteristics. Furthermore, the layered structure of coal, along with its natural microcracks and micropores, is well developed. The evolution of microscale pores and fractures during coal splitting in Brazil significantly affects macroscopic fracture morphology and is closely related to splitting failure characteristics (Feng et al., 2020). Most existing research focuses on the permeability, uniaxial compressive strength, and elastic modulus of coal after water immersion but does not adequately consider the combined effects of mine water immersion, bedding plane direction, and loading rate. Consequently, it is necessary to investigate the mechanical characteristics and resistance to splitting failure of coal under the influence of these factors in Brazil.

2. Coal samples and mechanical experiments

2.1. Coal samples

The coal sample used in this study is sourced from a major mining area in northwest China, which is identified as a potential site for constructing underground water reservoirs for coal mines. Intact coal specimens demonstrating structural homogeneity and absence of macroscopic discontinuities were selected for experimental investigation. The coal is collected from underground mines, as illustrated in Fig. 1. Coal predominantly consists of organic matter, along with minor amounts of minerals and other components. Initially, cylindrical samples measuring ϕ 50 × 100 mm were drilled in the direction parallel to and perpendicular to the bedding planes. Subsequently, the cylindrical specimens were cut into circular samples measuring ϕ 50 × 25 mm.

To evaluate the effect of bedding on coal splitting in Brazil, the angle (θ) between the applied force and the bedding plane direction was set to seven conditions: 0°, 15°, 30°, 45°, 60°, 75°, and 90°. Additionally, eight specimen types were examined with the applied force perpendicular to the bedding plane, as illustrated in Fig. 2. The configuration at $\theta = 0°$ is referred to as the Splitter-type, while the configuration at $\theta = 90°$ is termed the Arrester-type. When a load is applied perpendicular to the orthogonal bedding plane, this configuration is designated as the Divider-type.

2.2. Mine water immersion and brazilian splitting experiment

Mine water was collected from the underground reservoir of the coal mine, and coal samples were subsequently immersed in it. Different immersion durations were established at 0 days, 30 days, and 120 days. Following immersion in mine water, Brazilian splitting mechanical tests were promptly conducted on the coal samples. The experiments were performed using an INSTRON mechanical testing machine at Sichuan

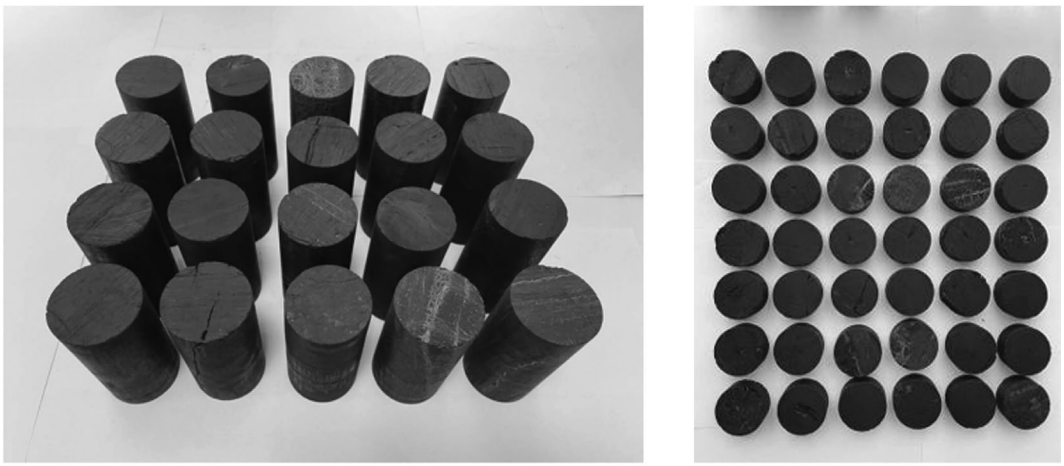

(a) Coal cylinder samples (b) Coal Brazilian disc samples

Fig. 1. Photos of partial coal samples.

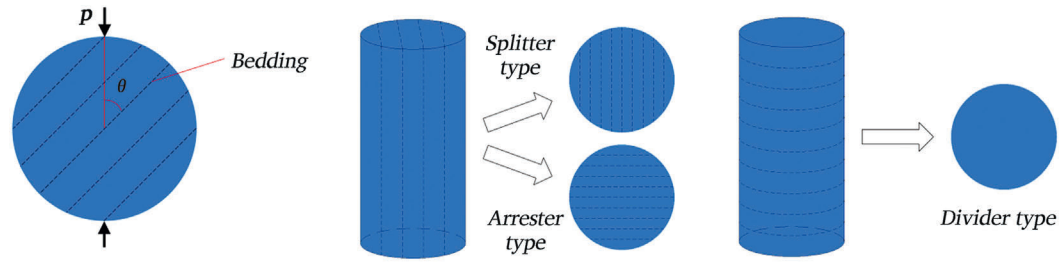

(a) Stratified plane dip angle (b) Splitter-type and Arrester type (c) Divider-type

Fig. 2. Schematic diagram of coal sample types.

University, with loading rates set to 0.005 kN/s, 0.02 kN/s, 0.05 kN/s, and 0.1 kN/s. Fig. 3 illustrates the Brazilian splitting mechanical test performed on coal.

Based on elasticity theory, the tensile strength during Brazilian splitting can be derived from the stress state at the center point of the disc (Feng et al., 2020; Wong et al., 2014). The tensile strength of coal rock can be calculated using the following formula (Gholami et al., 2014):

$$\sigma_t = \frac{2P_{\max}}{\pi BD} \tag{1}$$

In this context, σ_t represents the Brazilian splitting strength (MPa); $P_{\max}$ denotes the peak load (N); B indicates the thickness of the sample (mm); and D refers to the diameter of the sample (mm).

3. Experimental results and analysis

3.1. Brazilian splitting strength

Measure the dimensions of each coal sample, substitute the data into Eq. (1), and calculate the Brazilian splitting strength (*BSS*) for each sample, along with the average value obtained under the same conditions. The results of the calculations were plotted as curves, as illustrated in Figs. 4 and 5.

According to Fig. 4, the splitting strength of the Splitter-type coal samples prior to immersion was 0.74 MPa; after immersion for 30 days, it decreased to 0.36 MPa, representing a reduction of 51.35%. The Brazilian splitting strength of the Arrester-type coal sample before immersion was 1.39 MPa, which decreased to 0.76 MPa after 30 days of immersion, reflecting a decrease of 45.32%. For the Divider-type coal samples, the splitting strength was 1.86 MPa before immersion and reduced to 1.11 MPa after 30 days of immersion, indicating a decrease of 40.32%. Therefore, immerse in mine water significantly weakens the breakage resistance of various types of coal. This reduction may result from the damage inflicted by mine water on coal. As immersion time increases, the moisture content within the coal exhibits an exponential increase (Yao et al., 2020b). The weakening effect associated with changes in bond and non-bond energy can lead to a decrease in the mechanical strength of coal molecules (Jiao et al., 2024), promoting the continuous development and expansion of pores and fractures, gradually increasing the porosity of coal (Ai et al., 2021) and weakening its mechanical properties.

Fig. 5a illustrates that the Brazilian splitting strength (*BSS*) of coal exhibits a pattern of initially increasing, then decreasing, and subsequently increasing again with the dip angle of the bedding plane. The splitting strength increased from 0.36 MPa at $\theta = 0^\circ$ to 0.58 MPa at $\theta = 30^\circ$, reflecting a 61.11% increase. However, at $\theta = 45^\circ$, the *BSS* sharply decreased to a minimum value of 0.31 MPa, representing a 46.55% reduction, indicating that the coal has the weakest ability to resist splitting damage at this angle. Following this, the *BSS* gradually increased with the dip angle, reaching a maximum of 0.76 MPa at $\theta = 90^\circ$, a 145.16% increase compared to the value at $\theta = 45^\circ$, at which point the coal exhibits the strongest ability to resist splitting damage. This behavior is influenced by the mechanical structure defined by the direction of force and the bedding planes. Although the coal Brazilian disk samples do not exhibit pre-existing cracks, the weak planes along their natural bedding and microcracks significantly impair their resistance to crack propagation. This is influenced not only by the mechanical structure formed by applied loads and bedding planes but also by the effectiveness of bedding planes and microcracks in resisting unstable

Fig. 3. Schematic diagram of Brazilian splitting loading for coal samples.

expansion.

The Brazilian splitting strength (*BSS*) of coal at different loading rates was calculated using experimental data, with the results presented in Fig. 5b. As the loading rate increases, the *BSS* gradually rises. At $V =$ 0.005 kN/s, the average *BSS* is 0.49 MPa; at $V = 0.02$ kN/s, the average *BSS* value is 0.74 MPa; at $V = 0.05$ kN/s, the average *BSS* is 0.94 MPa; and at a loading rate of $V = 0.1$ kN, the average *BSS* reaches 1.06 MPa, representing a 117.81% increase compared to the lowest value. Despite the significant increase, the trend of the curve gradually flattens, which may be related to the speed of damage evolution in coal. A study by Li et al. (2016) demonstrated that as the loading rate increases, the rate of load application on the coal sample also accelerates, resulting in a negative correlation between damage stress and loading rate.

3.2. Brazilian splitting modulus

The elastic modulus is commonly used to assess the stress-strain relationship of rocks during the elastic deformation stage. In the Brazilian splitting experiment, the Brazilian splitting modulus (Yu et al., 2004) is defined from a dimensional perspective to indicate the ability of coal to resist elastic deformation. The vertical axis of the experimental force-displacement curve is normalized by the area of the rock's meridian plane, as shown in Eq. (2), while the horizontal axis is normalized by the diameter of the coal sample, as demonstrated in Eq. (3), resulting in a new curve. The slope of the straight segment of this new curve represents the Brazilian splitting modulus.

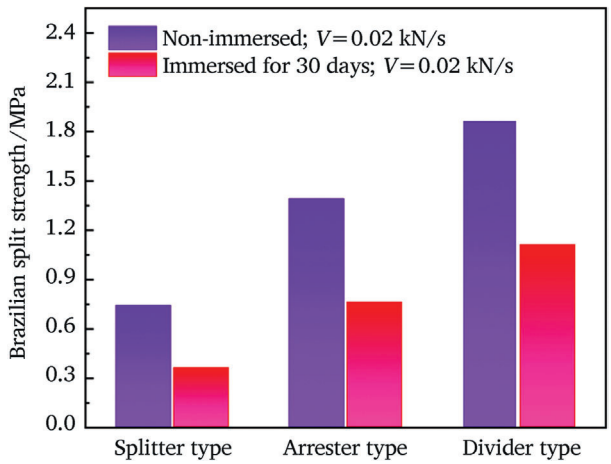

Fig. 4. Brazilian splitting strength of coal samples before and after immersion.

$$Y_2 = \frac{Y_1}{S_m} \tag{2}$$

$$X_2 = \frac{X_1}{D} \tag{3}$$

In this context, Y_1 represents the vertical axis (N) of the original force-displacement curve, while X_1 denotes the horizontal axis (mm) of the original force-displacement curve. Similarly, Y_2 represents the vertical axis (N) of the new load-displacement curve, and X_2 indicates the horizontal axis (mm) of the new force-displacement curve. Additionally, S_m refers to the thickness of the sample (mm), and D represents the diameter of the sample (mm). The variation trend of Brazilian splitting modulus is shown in Fig. 6.

As illustrated in Fig. 6a, after immerse in mine water, the trend of the Brazilian splitting modulus of coal closely aligns with that of the Brazilian splitting strength, both exhibiting fluctuations with respect to the dip angle of the bedding plane. When the angle θ ranges from 0° to 60°, the Brazilian splitting modulus remains relatively low, varying between 80.12 MPa and 95.91 MPa, with its minimum occurring at $\theta = 45°$. At θ = 75° and 90°, the Brazilian splitting strength is notably higher, reaching a maximum of 129.49 MPa at $\theta = 90°$. Sun et al. (2025) also demonstrated that after immerse in water, the elastic modulus of coal displays significant anisotropic characteristics. Fig. 6b reveals that the Brazilian splitting modulus of coal gradually increases with the loading rate. The splitting modulus of coal improved significantly from 83.65 MPa at $V = 0.005$ kN/s to 114.86 MPa at $V = 0.002$ kN/s, representing a 37.31% increase. However, at higher loading rates, the changes are more moderate; for instance, at $V = 0.1$ kN/s, the Brazilian splitting modulus reaches 136.07 MPa, an increase of only 18.46% compared to $V = 0.002$ kN/s.

3.3. Absorbed energy

The deformation and failure processes of coal and rock are accompanied by the absorption, accumulation, and dissipation of energy. Examining the energy dynamics that govern the failure of coal and rock can provide a more comprehensive understanding of their mechanical behavior (Wasantha et al., 2014). The energy absorbed by the coal sample until failure is termed absorbed energy (Tavallali et al., 2010). Estimating absorbed energy parallels the methodology employed in uniaxial compressive strength experiments. By calculating the area between the curve and the *x*-axis in the experimental force-displacement

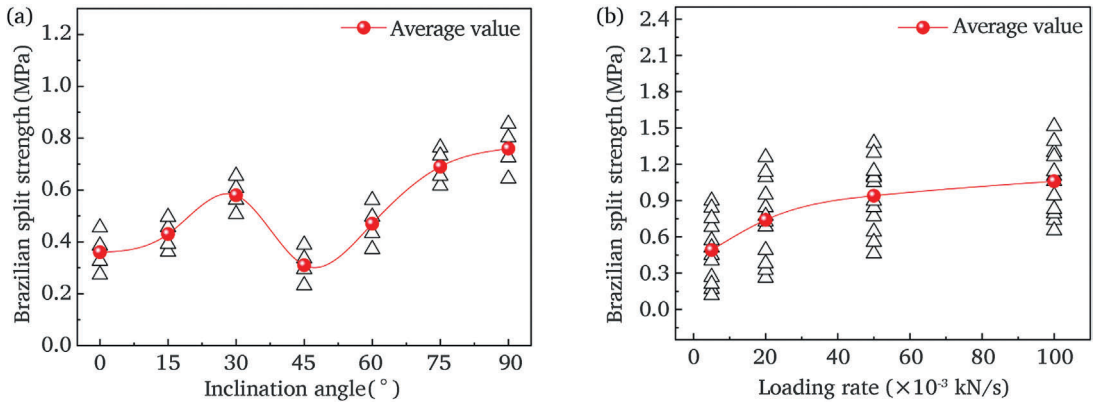

Fig. 5. Variation curve of the Brazilian splitting strength (*BSS*) for coal samples ((a)-Variation in *BSS* with inclination angle (θ) at a loading rate of $V = 0.02$ kN/s; (b)-Variation in *BSS* with loading rate (V)).

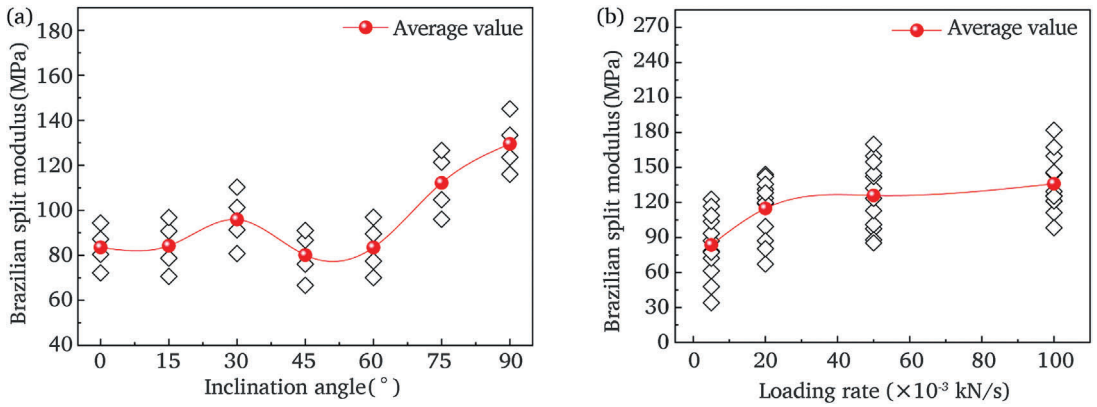

Fig. 6. Variation curve of the Brazilian splitting modulus (E_m) for the coal sample ((a) Variation in E_m with inclination angle (θ) at a loading rate of $V = 0.02$ kN/s; (b) Variation in E_m with loading rate (V)).

curve, the absorbed energy (U_a) can be derived, as illustrated in Eq. (4) (Hou et al., 2016).

$$U_a = \int_0^{L_k} P_k \cdot \mathrm{d}l \tag{4}$$

Among these parameters, U_a represents the absorbed energy (mJ), P_k denotes the load at time k (N), dl signifies the displacement difference (mm) between time k and k+1, and L_k indicates the displacement value at time k. The trend of Absorbed energy is shown in Fig. 7.

As indicated in Fig. 7a, the absorbed energy of coal immersed in mine water increased from 150.37 mJ at $\theta = 0°$ to 215.00 mJ at $\theta = 30°$. However, at $\theta = 45°$, the absorbed energy abruptly decreases, reaching its minimum value. As θ continues to increase from 45° to 90°, the absorbed energy rises significantly, reaching its maximum value of 304.74 mJ at $\theta = 90°$. As illustrated in Fig. 7b, the absorbed energy increases progressively with the loading rate. At loading rates of $V =$ 0.005 kN/s, 0.02 kN/s, 0.1 kN/s, and 0.5 kN/s, the corresponding absorbed energy values are 177.59 mJ, 275.38 mJ, 365.82 mJ, and 414.00 mJ, respectively. Initially, as the loading rate increases, the absorbed energy rises significantly. However, as the loading rate continues to increase, the trend in energy absorption changes more gradually.

The Brazilian splitting modulus and absorbed energy of non-immersion coal are 175.41 MPa and 271.40 mJ, respectively. Immersion in mine water reduces these parameters by 52.37% and 44.60%, respectively. A comparison of Figs. 5–7 indicates that the trends of coal energy absorption, Brazilian splitting strength, and Brazilian splitting modulus in relation to changes in bedding angle and loading rate are consistent, regardless of whether the coal is immersed in mine water. It is important to note that in the construction and operation of underground water reservoirs in coal mines, the width and height of coal pillars, the materials used for reinforcement, the reinforcement processes, and the support technologies must be rationally designed. Moreover, when developing these parameters and technologies, the tensile strength and energy absorption of coal should be considered. Therefore, it is essential to statistically analyze the relationship between splitting strength and absorbed energy, as illustrated in Fig. 8.

The relationship between the Brazilian splitting strength (*BSS*) and absorbed energy (U_a), as derived from the data presented in Fig. 8, is described by the equation $y = 0.0026x + 0.00235$ ($R^2 = 0.8410$). This analysis reveals a positive correlation between splitting strength and energy absorption in Brazilian coal, indicating that an increase in splitting force leads to greater energy absorption during the destabilization of the coal pillar.

4. Discussion

Coal is a geological formation characterized by distinct bedding resulting from sedimentation under specific geological conditions. This resource is rich in organic matter, while mine water contains complex ions. The prolonged interaction between coal and mine water inevitably alters the composition and structure of the coal. Microscopic pores and fractures significantly influence the macroscopic mechanical response characteristics of coal by affecting the mechanical structure formed by the coal matrix, layer properties, and layer orientation.

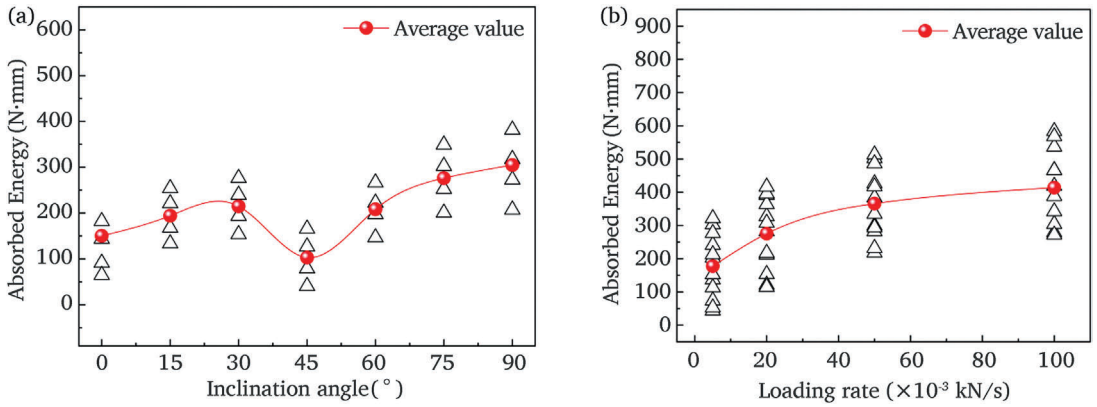

Fig. 7. Variation curve of absorbed energy during the Brazilian splitting test for the coal sample ((a) Variation in absorbed energy with the inclination angle (θ) at a loading rate of $V = 0.02$ kN/s; (b) Variation in absorbed energy (U_a) with the loading rate (V)).

4.1. The influence of mine water immersion on micro pore cracks

Certain minerals in coal are prone to softening in the presence of water. In contrast to pure water, mine water is a complex aqueous solution that typically exhibits varying levels of acidity, alkalinity, or high salinity. Prolonged exposure to acidic conditions increases the porosity, fracture opening, permeability, and overall deterioration of rocks (Sheng et al., 2012). The effects of chemical corrosion on rock crack propagation are complex and depend on various factors, including the composition and concentration of chemical ions in the solution, pH, the extent of existing cracks, and the mineral composition of the rock (Chen et al., 2003; Han et al., 2019). Previous studies employing biochemical, physical, and chemical methods (Sapsford et al., 2015; Zhao and Sun et al., 2019b; Iakovleva et al., 2016; Rakotonimaro et al., 2017) have shown that mine water may contain heavy metals and organic compounds, including ions such as Fe^{3+}, Ca^{2+}, Cu^{2+}, Na^{+}, Cr^{6+}, Mg^{2+}, K^{+}, S^{2-}, NO_3^-, NO_2^-, NH^{4+}, SO_4^{2-}, HCO_3^-, H^{+}, Cl^{-} Ions, etc. Clay minerals, calcite, sulfides, hydroxides, and sulfate minerals in coal are susceptible to chemical reactions like dissolution when exposed to high concentrations of saline solutions. The damage caused to coal can be substantial. To quantify the impact of mine water immersion on the microscopic characteristics of coal, low-temperature nitrogen adsorption experiments were conducted. Fig. 9 illustrates the low-temperature nitrogen adsorption and desorption isotherm of coal.

According to the Brunauer-Deming-Deming-Teller (BDDT) classification (Perera et al., 2013) and the International Union of Pure and Applied Chemistry (IUPAC) classification (Sing et al., 1985), the low-temperature nitrogen adsorption-desorption isotherm of the tested coal is classified as type IV, exhibiting a H4 hysteresis loop. This observation indicates that the pore geometry in coal predominantly consists of narrow slit-shaped pores. The minimal variation in the shape of the hysteresis loop suggests that the immerse in mine water has little effect on the geometric configuration of coal pores. The pore structure parameters of coal samples affected by immerse in mine water were determined through adsorption isotherms, as illustrated in Figs. 10 and 11.

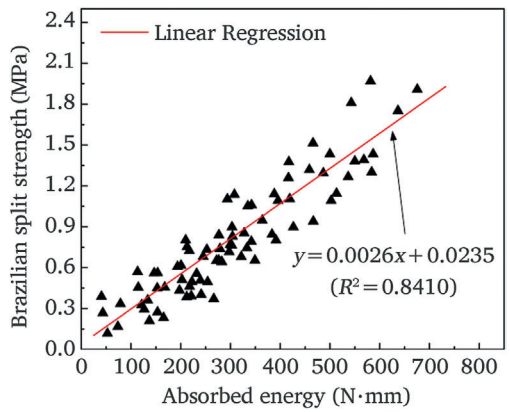

Fig. 8. Relationship curve between *BSS* and U_a of coal samples.

Damage refers to the degradation process of materials resulting from microstructural defects, such as microcracks and voids, under external loads and environmental conditions. Changes in microstructure lead to the accumulation of damage, which is reflected in the macroscopic mechanical response of coal, affecting its mechanical properties and failure characteristics. According to Fig. 10a, as the immersion time in mine water increases, the specific surface area of the coal sample gradually rises from 4.2717 m^2/g (untreated) to 12.5705 m^2/g after 120 days of immersion. The leaching effect of mine water reduces the mineral content of coal and increases its surface energy. Simultaneously, the total pore volume of coal increases, as shown in Fig. 10b, from 0.0126 cm^3/g (untreated) to 0.0180 cm^3/g after immersion. Mine water causes partial dissolution of components in coal samples, resulting in a decrease in the volume of solid parts and an increase in the volume of formed pores. It was observed that the average pore size of coal significantly decreased from 11.7986 nm (untreated) to 5.7277 nm after 120 days of water immersion, as shown in Fig. 10c, representing a decrease of 51.45%. This indicates that mine water not only induces coal cracking but also disperses and distributes the cracked particles. Furthermore, the rate at which mine water increases the specific surface area exceeds the rate of total pore volume increase. From the proportion of pore volume within each pore size range, as illustrated in Fig. 10d, as the immersion time in mine water increases, the proportion of micropores (<2 nm) and small pores (2–10 nm) gradually rises, while the proportion of mesopores (10–50 nm) and macropores (50–200 nm) gradually decreases. This trend indicates that mine water immersion leads to the emergence of a significant number of micropores and small pores in coal, with the increase rate of these pores surpassing their conversion rate to mesopores and macropores.

Fig. 11 illustrates the pore size distribution of the coal sample, derived from the N_2 desorption isotherm. The pore size distribution curves for untreated coal samples, water-immersed coal samples for 30 days, and water-immersed coal samples for 120 days exhibit a unimodal characteristic, with peaks at pore sizes of 3.9426 nm, 3.9828 nm, and 3.9800 nm, respectively, within the range of 2–10 nm. The peak following immersion is higher than that of the untreated sample, indicating an increase in the proportion of small pores. The curve for pores smaller than 2 nm is also higher after water immersion compared to the untreated samples, indicating a significant increase in the proportion of micropores. This suggests that the mineral dissolution mechanism, resulting from interactions between mine water and coal components,

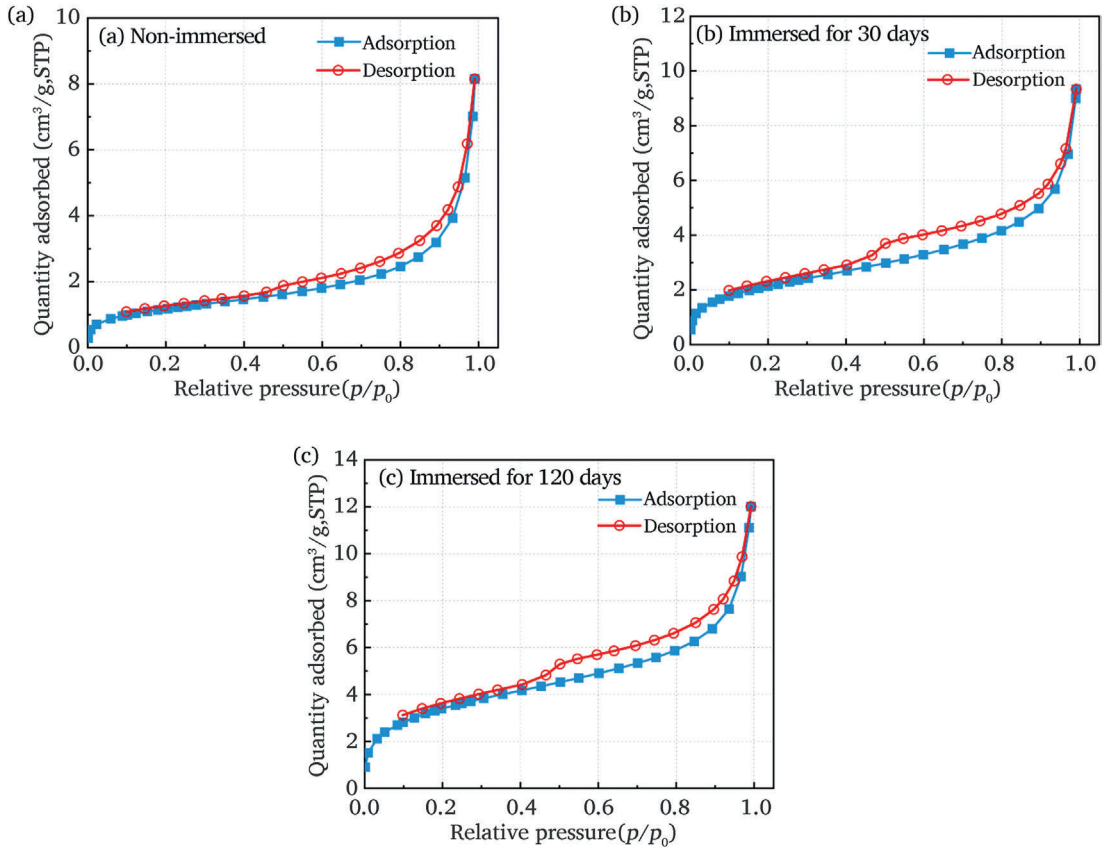

Fig. 9. Low temperature N_2 adsorption-desorption isotherms of coal samples.

occurs not only around the particles but also within them. The predominant mechanism of mineral particle cracking surpasses that of water absorption and expansion. The fractured coal skeleton exhibits a dispersed structure, characterized by numerous micropores, while macropores and mesopores increase in size at a relatively slower rate, thereby affecting the mechanical properties of coal to some extent. A study by Sun et al. (2022, 2023) indicated that the specific surface area and total pore volume of bituminous coal after CO_2 adsorption were lower than those of untreated samples, which also showed a decrease in strength. Conversely, Jin et al. (2020) found that the specific surface area, total pore volume, and average pore size of rocks increase with rising heat treatment temperatures, attributing the increase in pore and fracture size to the reduction in rock strength. Thus, it is evident that while different environments (mine water immersion, CO_2 immersion, high-temperature heat treatment) induce changes in the mechanical properties of coal and rock, the micro-mechanisms of action are not entirely the same.

To visually observe the distribution of pores and fractures, as well as the micropores and small pores in coal affected by mine water immersion, scanning electron microscopy (SEM) was employed. This method allows for the examination of the evolutionary process of these features developing into larger pores and fractures, as illustrated in Fig. 12.

Coal is predominantly composed of organic matter, with minor minerals, metals, and other substances; its elemental composition exceeds 98% C and O (Fig. 12a). Certain organic and mineral components undergo physical and chemical reactions with water. non-immersed coal contains intrinsic pores and fractures (Fig. 12b). After 30 days of mine water immerse, surface crack dimensions increase markedly (Fig. 12c), demonstrating structural degradation caused by aqueous interactions. Prolonged immerse exponentially elevates coal's water content, driving pore expansion (Yao et al., 2020b). These results suggest that component dissolution in aqueous mine water environments-where dissolution rates exceed particle swelling from water absorption-contributes to structural weakening. Ahamed et al. (2019) attributed reduced coal strength to solvent effects, wherein water molecules aggregate around polar functional groups and accumulate in clay minerals. Carbonate dissolution in water further diminishes interparticle stress, lowering mechanical strength. Fig. 12d illustrates surface corrosion perpendicular to coal bedding planes, with fractures propagating along bedding layers. Water infiltrates coal through these planes, inducing skeletal degradation and progressive enlargement of pre-existing bedding-plane fractures. Fig. 12e reveals that after 120 days of immerse, coal pores and fractures coalesce into fragmented structures, with large fractures undergoing significant expansion-collectively driving severe structural disintegration. Pore connectivity facilitates pore network formation, culminating in interconnected fracture-pore zones (Fig. 12f), ultimately resulting in a loosened coal matrix. These fractured and interconnected regions significantly diminish coal's load-bearing capacity, directly impairing its mechanical properties.

Based on the analysis of physical and chemical reactions, low-temperature nitrogen adsorption experiments, and scanning electron microscopy (SEM) observations, it can be concluded that the interaction between mine water and coal induces changes in the clay mineral composition of coal. The reduction in coal composition is greater than the addition of newly generated components, resulting in an increase in coal pores and cracks. While mine water creates various scales of pores and fractures in coal, its effect on promoting the formation of numerous micropores and small pores is more pronounced. The generation rate of these micropores and small pores exceeds their conversion rate to mesopores and macropores. This mechanism of pore and fissure evolution leads to the formation of fragmented coal structures, weakening the interconnections among the internal components of coal, a process that intensifies with prolonged mine water immersion. Concurrently, pores and fractures progressively converge and merge, facilitating the

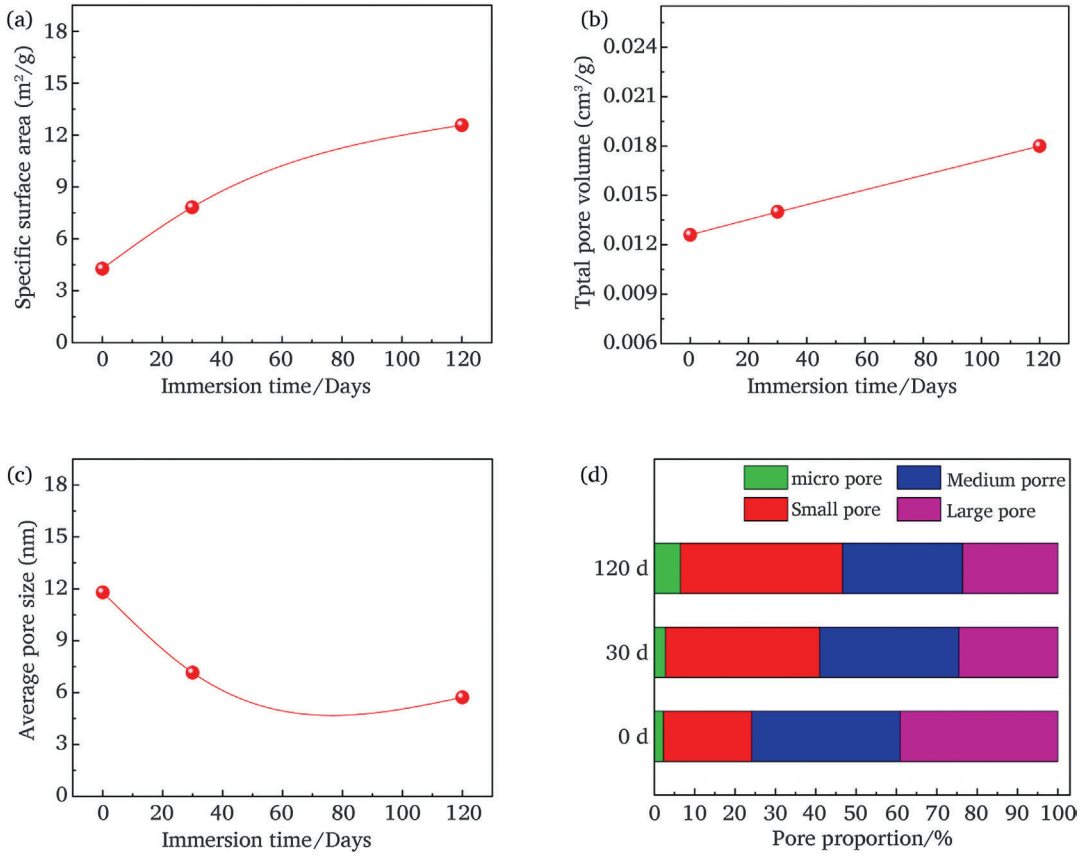

Fig. 10. Pore structure parameters of coal samples.

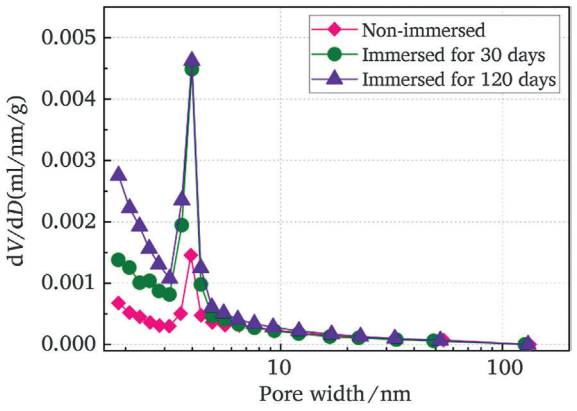

Fig. 11. Pore size distribution of coal under different immersion durations in mine water.

connection between fragmented structures and forming a zone of interconnected pores and fractures. Ultimately, the fragmented structure and the interconnected zone of pores and cracks contribute significantly to a decrease in the coal's bearing capacity.

4.2. Impact of bedding-plane structures on coal's mechanical properties

The load and bedding direction create a mechanical structure, with its stability varying according to the bedding angle. Under different bedding angles, the failure modes of rocks will differ (Jin et al., 2020). When subjected to sufficient stress and deformation, coal will develop cracks. The formation of these cracks is a mechanical manifestation of changes in the stability of the structural integrity. The load applied to coal can be decomposed into normal stress perpendicular to the bedding plane and shear stress parallel to the bedding plane, as illustrated in Fig. 13.

As the inclination angle θ changes from 0° to 90°, both the magnitude and direction of normal and shear stress vary (Feng et al., 2019; 2020). The stress distribution governs the failure characteristics. Failure under Brazilian splitting is not solely characterized by pure tensile failure; it can also involve pure shear failure, and in many cases, it manifests as a composite failure mode of tensile and shear (Debecker et al., 2013). In this study, coal affected by mine water immersion demonstrates distinct mechanical properties and fracture characteristics. At $\theta = 0°$ and 90°, the primary crack propagates vertically along the center position. This occurs because the load is aligned with or perpendicular to the bedding plane, resulting in a largely symmetrical stress structure in the coal. Under vertical loading, coal experiences uniform tensile stress that extends laterally. At $\theta = 15°$ and 30°, most of the primary fractures continue to propagate along the bedding plane. At $\theta = 45°$, a mechanical structure conducive to shear sliding along the bedding plane is established, making coal particularly susceptible to fracture. As θ increases to 60° and 75°, the proportion of the matrix that must be overcome for coal fracture rises, leading to a significant increase in splitting strength and exhibiting a combination of shear and tensile fracture properties. The failure mode of coal is heavily influenced by the angle between the bedding plane and the loading direction, and is closely related to the properties of the bedding planes and matrix of the coal. Under pressure, coal undergoes lateral deformation due to the Poisson effect; the weaker the bedding plane, the more pronounced the force effect generated along the weak plane.

At $\theta = 0°$ (Splitter-type), tensile fractures predominantly propagate along the bedding plane, reflecting the bedding's tensile strength. At $\theta = 90°$ (Arrester-type), tensile stress concentrates within the matrix, highlighting the matrix's tensile strength. The coal sample exhibits pronounced bedding-plane defects with lower strength relative to the

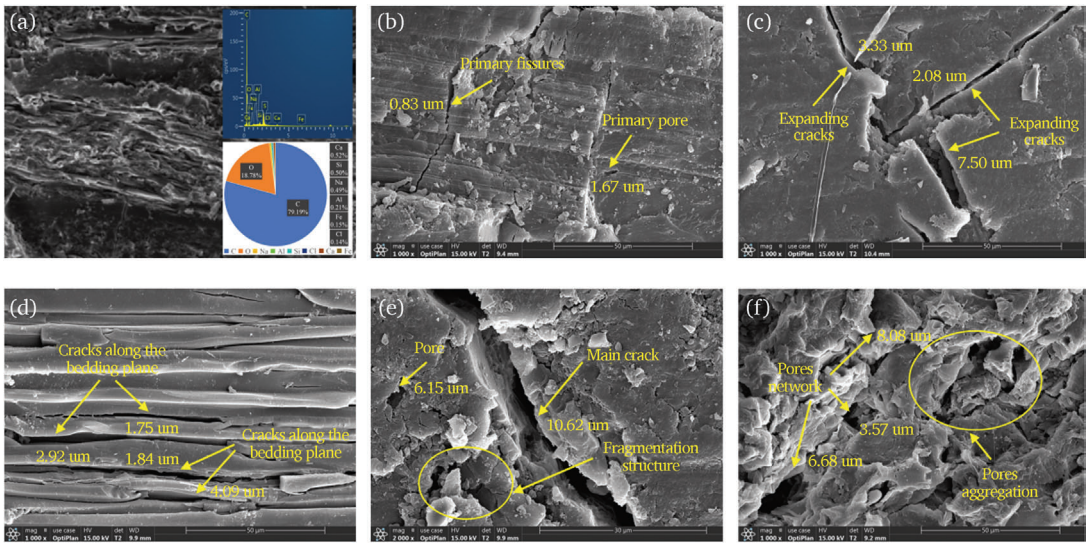

Fig. 12. Scanning electron microscopy observation images of coal samples ((a) proportion of coal EDS elements; (b) no immerse; (c) immersed for 30 days; (d) layered cracks; (e) Cracks after immersion for 120 days; (f) Pores immersed for 120 days).

matrix, resulting in Splitter-type *BSS* values being lower than Arrester-type values. For Divider-type samples, fracture necessitates overcoming both bedding-perpendicular mechanical structures and the matrix itself. This hybrid tensile-compressive stress regime demands greater energy input, yielding Divider-type *BSS* values exceeding those of Arrester-type samples.

Through the analysis of the mechanical structure, fracture trajectory, and fracture characteristics of coal, it can be concluded that the mechanical properties of coal vary under different bedding angles (θ). As the bedding angle θ changes from 0° to 90°, both the magnitude and direction of normal and shear stress also change. The distribution of stress determines the failure characteristics of coal. These destructive characteristics directly lead to differences in the mechanical properties and fracture patterns of coal. The fundamental reason for this variation lies in the relative proportion of failure mechanisms occurring along and across the bedding plane, which directly influences the mechanical properties of coal at different θ values. A greater occurrence of fracture mechanisms along the bedding plane results in weaker mechanical properties, indicating a reduced ability of coal to resist fracture. In contrast, the mechanism of cross-layer damage enhances the mechanical properties of coal. Notably, the Brazilian splitting strength of coal remains consistent with changes in bedding angle and loading type, both in untreated samples and those subjected to mine water immersion. This indicates that the cracking mechanisms of the coal matrix and bedding plane are similar under mine water immersion.

4.3. Loading rate effects on coal fracture behavior in the brazilian test

The loading rate critically governs the mechanical properties of coal. As shown in Fig. 5b, Brazilian splitting strength (*BSS*) exhibits a positive correlation with loading rate. To quantify this relationship, logarithmic loading rate (lg*V*) was plotted against *BSS* (Fig. 14).

Therefore, data fitting was performed on the average *BSS* values of the Splitter-type, Arrester-type, and Divider-type, and Eqs. (5)–(7) based on linear regression results were obtained.

$$\text{Splitter type}: y = 0.4393x + 1.1694, \left(R^2 = 0.9713\right) \tag{5}$$

$$\text{Arrester type}: y = 0.4573x + 1.5377, \left(R^2 = 0.9941\right) \tag{6}$$

$$\text{Divider type}: y = 0.4375x + 1.8140, \left(R^2 = 0.9982\right) \tag{7}$$

Among them, x represents the logarithm of the loading rate (lg*V*),

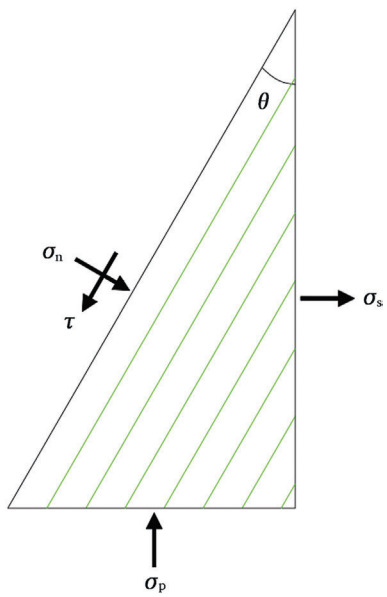

Fig. 13. Schematic diagram of stress decomposition under different θ

and y represents the Brazilian splitting strength (*BSS*).

A higher loading rate reduces crack damage, enhancing load-bearing capacity; however, it increases elastic energy storage in microstructural elements, inducing localized damage (Li et al., 2015). Coal inherently contains natural pores and cracks, with new cracks nucleating under external loads. At low loading rates, microcracks coalesce into macroscopic fractures, while high rates reduce the likelihood of defect coalescence into larger cracks. The dominant crack preferentially aligns with the applied stress direction (Zhu et al., 2021). Increased loading rates expedite damage propagation, accelerating the transition from internal damage to macroscopic failure (Li et al., 2016). Higher loading rates induce earlier damage stress initiation, and specimen failure occurs more rapidly. Consequently, coal fragmentation necessitates overcoming greater resistance, enhancing its mechanical properties. Increasing loading rates correlate with higher coal strength, requiring greater fracture loads and energy absorption.

5. Conclusion

This article presents a series of experiments involving varying durations of mine water immersion, Brazilian splitting mechanics tests, and micro-pore crack observations on coal. It investigates the influence of bedding angle and loading rate on the mechanical response characteristics of coal under the effects of mine water immersion. The main conclusions are as follows.

(1) After soaking in mine water for 30 days, the Brazilian splitting strength (*BSS*), splitting modulus (E_m), and absorbed energy (U_a) were 0.36 MPa, 83.54 MPa, and 150.37 mJ, respectively, representing decreases of 51.35%, 52.37%, and 44.60% compared to untreated conditions. The leaching effect of mine water results in coal exhibiting ductile failure characteristics. This occurs due to the physical and chemical interactions among various substances within the mine water immersion environment, which compromise the structural integrity of the coal. The leaching effect increases coal porosity and the formation of fractures, leading to a significant number of micropores and small voids, with their formation rate exceeding the rate of transformation into mesopores and macropores. This results in the development of fragmented structures within the coal, and as the duration of mine water action increases, the connections between these fragmented structures form interconnected zones of pores and fractures. Ultimately, these fragmented structures and interconnected zones severely weaken the coal's bearing capacity.

(2) Under the influence of mine water immersion, the Brazilian splitting strength (*BSS*) values at bedding angles (θ) of 0°, 15°, 30°, 45°, 60°, 75°, and 90° are 0.36, 0.43, 0.58, 0.31, 0.47, 0.69, and 0.76 MPa, respectively. Within the range of $0° \leq \theta \leq 90°$, the *BSS*, splitting modulus (E_m), and absorbed energy (U_a) reach their maximum at $\theta = 90°$. Conversely, at $\theta = 45°$, these mechanical parameters are minimized due to the activation of layer shear fracture. The mechanical properties of coal exhibit a similar trend with changes in loading type, irrespective of mine water immersion effects. The relative proportion of failure mechanisms occurring along and across the bedding plane directly determines the mechanical properties of coal at different θ values. A greater occurrence of failure mechanisms along the bedding plane results in weaker mechanical properties, while mechanisms that break through the bedding plane enhance the mechanical properties of coal. Additionally, under vertical orthogonal loading, the Divider type exhibits the highest splitting strength and strongest resistance to fracture. The impact of mine water immersion on the bedding planes and matrix of the three sample types (Splitter-type, Arrester-type, and Diver-type) is generally consistent. These changes are related to the mechanical structure (magnitude and direction of stress); specifically, the mechanical structure, bedding properties, and matrix characteristics of coal jointly determine its failure characteristics.

(3) At loading rates of 0.005 kN/s, 0.02 kN/s, 0.05 kN/s, and 0.1 kN/s, the Brazilian splitting strength (*BSS*) values were 0.49 MPa, 0.74 MPa, 0.94 MPa, and 1.06 MPa, respectively. The splitting modulus (E_m) values were 83.65 MPa, 114.86 MPa, 126.02 MPa, and 136.07 MPa, respectively. The absorbed energy (U_a) values were 177.59 mJ, 275.38 mJ, 365.82 mJ, and 414.00 mJ, respectively. Notably, the different loading rates did not alter the relative order of the mechanical properties of the three coal sample types (Diverter-type > Arrester-type > Splitter-type). As the loading rate increases, *BSS*, E_m, and U_a all gradually rise, although the increase is gentle. This is primarily because the increase in loading rate shortens the time available for the development and evolution of internal damage in coal, thereby reducing the likelihood of activating weak structures within the coal. Consequently, this results in greater resistance to the propagation of fracture cracks in the direction of the applied load.

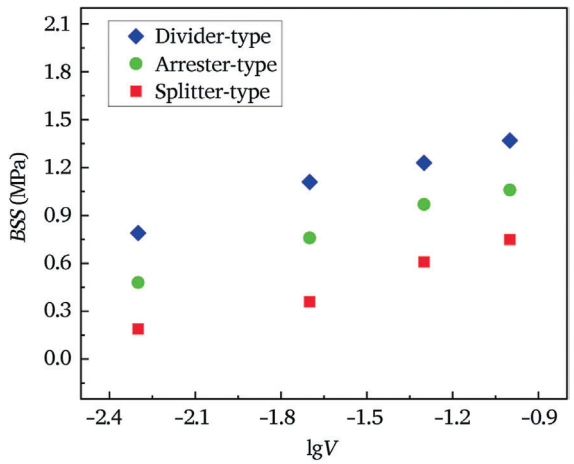

Fig. 14. The trend of coal *BSS* changes with lg*V*.

This study is highly significant for optimizing the design and evaluating the safe operation of coal pillars in underground water reservoirs of coal mines.

CRediT authorship contribution statement

Xiaobin Li: Writing – original draft, Data curation, Conceptualization. **Gan Feng:** Writing – original draft, Methodology, Data curation, Conceptualization. **Xu Wang:** Writing – review & editing, Methodology, Investigation. **Jianxiong Yang:** Methodology, Investigation, Formal analysis. **Yu Zhao:** Writing – original draft, Resources, Formal analysis. **Guifeng Wang:** Writing – review & editing, Formal analysis, Conceptualization. **Mingli Xiao:** Writing – review & editing, Formal analysis, Data curation, Conceptualization. **Chunyu Gao:** Writing – review & editing, Writing – original draft, Investigation. **Huaizhong Liu:** Writing – review & editing, Methodology, Investigation.

Declaration of competing interest

The authors declare the following financial interests/personal relationships which may be considered as potential competing interests: Xu Wang is currently employed by China Railway Chuanzang Science and Technology Innovation Center (Chengdu) Co., Ltd. and Sichuan Tibet Railway Technology Innovation Center Co., Ltd.

Acknowledgements

This study were supported by the National Natural Science Foundation of China (Grant No. 52374099; 52404109), the open fund of State Key Laboratory of Water Resource Protection and Utilization in Coal Mining (Grant No. GJNY-21-41-01), and the Natural Science Foundation of Sichuan Province, China (Grant No. 2025YFHZ0323) which are greatly appreciated.

References

Ahamed, M.A.A., Perera, M.S.A., Matthai, S.K., Ranjith, P.G., Li, D.Y., 2019. Coal composition and structural variation with rank and its influence on the coal-moisture interactions under coal seam temperature conditions—A review article. J. Petrol. Sci. Eng. 180, 901–917.

Ai, T., Wu, S., Zhang, R., Gao, M., Zhou, J., Xie, J., Ren, L., Zhang, Z., 2021. Changes in the structure and mechanical properties of a typical coal induced by water immersion. Int. J. Rock. Mech. Min. 138, 104597.

Bodeux, S., Pujades, E., Orban, P., Brouyère, S., Dassargues, A., 2017. Interactions between groundwater and the cavity of an old slate mine used as lower reservoir of

an UPSH (Underground Pumped Storage Hydroelectricity): A modelling approach. Eng. Geol. 217, 71–80.
Bussar, C., Stocker, P., Cai, Z., Moraes, L., Magnor, D., Wiernes, P., Moser, A., Bracht, N., Sauer, D., 2016. Large-scale integration of renewable energies and impact on storage demand in a European renewable power system of 2050 sensitivity study. J. Energy Storage 6, 1–10.
Chen, S.L., Feng, X.T., Li, S.J., 2003. Effects of chemical erosion on uniaxial compressive strength and meso-fracturing behaviors of rock. Chin. J. Rock Mech. Eng. 22 (4), 547–551.
Chen, T., Yao, Q., Ju, M., Liang, S., Liu, Y., Li, X., 2017. Effects of water intrusion and loading rate on mechanical properties of and crack propagation in coal–rock combinations. J. Central. South. Univ. 24 (2), 183–191.
Colas, E., Klopries, E.M., Tian, D., Kroll, M., Selzner, M., Bruecker, C., Khaledi, K., Kukla, P., Preuße, A., Sabarny, C., Schüttrumpf, H., Amann, F., 2023. Overview of converting abandoned coal mines to underground pumped storage systems: Focus on the underground reservoir. J. Energy Storage 73, 109153.
Debecker, B., Vervoort, A., 2013. Two-dimensional discrete element simulations of the fracture behaviour of slate. Int. J. Rock Mech. Min. Sci. 61, 161–170.
Feng, G., Kang, Y., Sun, Z.D., Wang, X.C., Hu, Y.Q., 2019. Effects of Supercritical CO2 adsorption on the mechanical characteristics and failure mechanisms of shale. Energy 173, 870–882.
Feng, G., Kang, Y., Wang, X.C., Hu, Y.Q., Li, X.H., 2020. Investigation on the failure characteristics and fracture classification of shale under Brazilian test conditions. Rock Mech. Rock Eng. 53 (7), 3325–3340.
Gholami, R., Rasouli, V., 2014. Mechanical and elastic properties of transversely isotropic slate. Rock Mech. Rock Eng. 47 (5), 1763–1773.
Han, T.L., Shi, J.P., Chen, Y.S., Cao, X.S., 2019. Mechanism damage to mode-I fractured sandstone from chemical solutions and its correlation with strength characteristic. Pure Appl. Geophys. 176 (11), 5027–5049.
Hou, P., Gao, F., Yang, Y.G., Zhang, Z.Z., Zhang, X.X., 2016. Effect of bedding orientation on failure of black shale under Brazilian tests and energy analysis. Chin. J. Geotech. Eng. 38 (5), 930–937 (in Chinese).
Hu, Y., Bie, Z., Ding, T., Lin, Y., 2016. An NSGA-II based multi-objective optimization for combined gas and electricity network expansion planning. Appl. Energy 167, 280–293.
Iakovleva, E., Maydannik, P., Ivanova, T.V., Sillanpää, M., Tang, W.Z., Mäkilä, E., Salonen, J., Gubal, A., Ganeev, A.A., Kamwilaisak, K., Wang, S.B., 2016. Modified and unmodified low-cost iron-containing solid wastes as adsorbents for efficient removal of As(III) and As(V) from mine water. J. Clean. Prod. 133, 1095–1104.
Jiao, L.F., Hao, C.Y., Duan, D., Lu, W.D., Gan, Y.P., Qi, J.J., Yang, W.R., Chen, Y.K., 2024. Molecular dynamics simulation of water absorption and mechanical weakening in coal rocks based on Monte Carlo methods. Solid State Ionics 418, 116743.
Jin, P.H., Hu, T.Q., Shao, J.X., Liu, Z.J., Feng, G., Song, S., 2020. Influence of temperature on the structure of pore–fracture of sandstone. Rock Mech. Rock Eng. 53, 1–12.
Kong, X.S., Yang, W., Shan, R.L., Wang, S., Fang, J., 2024. Ultimate water level and deformation failures of the artificial dam in the coal mine underground reservoir. Eng. Failure Anal. 162, 108367.
Li, H.T., Jiang, C.X., Jiang, Y.D., Wang, H.W., Liu, H.B., 2015. Mechanical behavior and mechanism analysis of coal samples based on loading rate effect. J. China Univ. Min. Technol. 44 (3), 430–436.
Li, Y.W., Jiang, Y.D., Yang, Y.M., Zhang, K.X., Ren, Z., Li, H.T., Ma, Z.Q., 2016. Research on loading rate effect of uniaxial compressive strength of coal. J. Min. Saf. Eng. 33 (4), 754–760 (in Chinese).
Ling, S.X., Wu, X.Y., Liao, X., Li, X.N., Zhao, S.Y., 2015. Study on the water-rock interaction behavior of xigeda strata in lamaxi gully, sichuan Province, China. Eng. Geol. Soc. Territory. 2, 2107–2111.
Liu, T.Y., Cao, P., 2016. Testing study of subcritical crack growth mechanism during water rock interaction. Geotech. Geol. Eng. 34 (4), 923–929.
Maruvanchery, V., Kim, E., 2019. Effects of water on rock fracture properties: studies of mode I fracture toughness, crack propagation velocity, and consumed energy in calcite-cemented sandstone. Geomech. Eng. 17 (1), 57–67.
Menéndez, J., Loredo, J., Galdo, M., Fernández-Oro, J.M., 2019. Energy storage in underground coal mines in NW Spain: assessment of an underground lower water reservoir and preliminary energy balance. Renew. Energy 134, 1381–1391.
Mileva, A., Johnston, J., Nelson, J.H., Kammen, D.M., 2016. Power system balancing for deep decarbonization of the electricity sector. Appl. Energy 162, 1001–1009.
Moriarty, P., Honnery, D., 2016. Can renewable energy power the future? Energy Policy 93, 3–7.
Okazaki, T., Shirai, Y., Nakamura, T., 2015. Concept study of wind power utilizing direct thermal energy conversion and thermal energy storage. Renew. Energy 83, 332–338.
Perera, M.S.A., Ranjith, P.G., Viete, D.R., 2013. Effects of gaseous and super–critical carbon dioxide saturation on the mechanical properties of bituminous coal from the Southern Sydney Basin. Appl. Energy 110, 73–81.
Qian, R.P., Feng, G.R., Liu, X.L., Yu, B., Ma, Q., Zeng, S.Y., Hu, N., Geng, H.L., 2024. Experimental investigation on mechanical and damage properties of single fractured coal subjected to water pressure and triaxial compression. Theor. Appl. Fract. Mech. 130, 104328.
Rakotonimaro, T.V., Neculita, C.M., Bussière, B., Zagury, G.J., 2017. Comparative column testing of three reactive mixtures for the bio-chemical treatment of iron-rich acid mine drainage. Miner. Eng. 111, 79–89.
Sadeghiamirshahidi, M., Vitton, S.J., 2019. Laboratory study of gypsum dissolution rates for an abandoned underground mine. Rock Mech. Rock Eng. 52 (7), 2053–2066.
Sapsford, D., Santonastaso, M., Thorn, P., Kershaw, S., 2015. Conversion of coal mine drainage ochre to water treatment reagent: production, characterisation and application for P and Zn removal. J. Environ. Manag. 160, 7–15.
Sheng, J.C., Li, F.B., Yao, D.S., Huang, Q.F., Song, H.B., Zhan, M.L., 2012. Experimental study of seepage properties in rocks fracture under coupled hydro-mechano-chemical process. Chin. J. Rock Mech. Eng. 31 (5), 1016–1025 (in Chinese).
Shi, X.S., Zhao, Y.X., Gong, S., Wang, W., Yao, W., 2022. Co-effects of bedding planes and loading condition on Mode-I fracture toughness of anisotropic rocks. Theor. Appl. Fract. Mech. 117, 103158.
Sing, K.S.W., Everett, D.H., Haul, R.A.W., Moscou, L., Pierotti, R.A., Rouquerol, J., Siemieniewska, T., 1985. Reporting physisorption data for gas/solid systems with special reference to the determination of surface area and porosity. Pure Appl. Chem. 57 (4), 603–619.
Song, H.H., Jiang, Y.D., Elsworth, D., Zhao, Y.X., Wang, J.H., Liu, B., 2018. Scale effects and strength anisotropy in coal. Int. J. Coal Geol. 195, 37–46.
Sun, Z.D., Feng, G., Song, X.M., Meng, T., Zhu, D.F., Huo, Y.M., Wang, Z.L., 2022. Effects of CO_2 state and anisotropy on the progressive failure characteristics of bituminous coal: an experimental study. Chin. J. Rock Mech. Eng. 41 (1), 70–81 (in Chinese).
Sun, Z.D., Xie, H.Q., Feng, G., Song, X.M., Chi, M.B., Meng, T., Sun, B.L., 2023. Effects of sub-/super-critical CO_2 on the fracture-related mechanical characteristics of bituminous coal. Front. Earth Sci. 3, 760–775.
Sun, Z.W., Zhang, R., Ren, L., Liu, X.L., Zhang, Z.P., Zha, E.S., Yang, X.Y., Liu, Z.H., Zhang, Z.T., 2025. Anisotropic mechanical properties of coal in a water-immersed pillar dam: insights from acoustic emission characterization. J. Rock Mech. Geotech. 17 (7), 4462–4475.
Tang, C.J., Yao, Q.L., Li, Z.Y., Zhang, Y., Ju, M.H., 2019. Experimental study of shear failure and crack propagation in water-bearing coal samples. Energy Sci. Eng. 1–12.
Tavallali, A., Vervoort, A., 2010. Effect of layer orientation on the failure of layered sandstone under Brazilian test conditions. J. Nat. Gas Sci. Eng. 47 (2), 313–322.
Wasantha, P., Ranjith, P.G., Shao, S.S., 2014. Energy monitoring and analysis during deformation of bedded-sandstone: use of acoustic emission. Ultrasonics 54 (1), 217–226.
Wong, L., Zou, C.J., Cheng, Y., 2014. Fracturing and failure behavior of carrara marble in quasistatic and dynamic Brazilian disc tests. Rock Mech. Rock Eng. 47 (4), 1117–1133.
Yang, K., Zhang, Z.N., Hua, X.Z., Liu, W.J., Chi, X.L., Lyu, X., Wang, Y., 2023. Microscopic mechanism of loading rate of saturated coal sample mechanics and damage characteristics. Coal Sci. Technol. 51 (2), 130–142 (in Chinese).
Yao, Q.L., Tang, C.J., Xia, Z., Liu, X.L., Zhu, L., Chong, Z.H., Hui, X.D., 2020a. Mechanisms of failure in coal samples from underground water reservoir. Eng. Geol. 267, 105494.
Yao, Q.L., Zheng, C., Tang, C.J., Xu, Q., Chong, Z.H., Li, X.H., 2020b. Experimental investigation of the mechanical failure behavior of coal specimens with water intrusion. Front. Earth Sci. 7, 348.
Yu, Y., Wang, T.X., 2004. Study on relationship between splitting behaviour and elastic modulus of three gorges granite. Chin. J. Rock Mech. Eng. 23 (19), 3258–3261 (in Chinese).
Zhang, L.Y., Zhang, S.J., Mao, X.B., Tang, X.Y., Qin, H., Li, B., Li, M., 2018. Experimental research of influence of loading rate on brittle-ductile transition of mudstone in coal rock strata. J. Min. Saf. Eng. 35 (2), 391–401 (in Chinese).
Zhang, S., Abdallah, K.B., Li, L., Hamdi, E., Liu, J., 2025. Multiphase flow controlled by synergistic injection-production pressure: enabling CO_2 geo-sequestration with additional gas recovery from vertically heterogeneous depleted shale reservoirs. Fuel 398, 135591.
Zhao, L., Sun, C., Yan, P.X., Zhang, Q., Wang, S.D., Luo, S.H., Mao, Y.X., 2019a. Dynamic changes of nitrogen and dissolved organic matter during the transport of mine water in a coal mine underground reservoir: Column experiments. J. Contam. Hydrol. 223, 103473.
Zhao, Y.X., Song, H.H., Liu, S.M., Zhang, C.G., Dou, L.M., Cao, A.Y., 2019b. Mechanical anisotropy of coal with considerations of realistic microstructures and external loading directions. Int. J. Rock. Mech. Min. Sci. 116, 111–121.
Zhu, C.Q., Li, S.B., Luo, Y., Guo, B., 2021. Progressive damage process and failure characteristics of coal under uniaxial compression with different loading rates. Shock Vib., 3360738